PERGAMON

Continental Shelf Research 22 (2002) 485–504

CONTINENTAL SHELF RESEARCH

www.elsevier.com/locate/csr

A high resolution tidal model for the area around The Lofoten Islands, northern Norway

H. Moe, A. Ommundsen, B. Gjevik*

Department of Mathematics, University of Oslo, Box 1053 Blindern, Oslo, Norway

Received 07 April 2000; received in revised form 19 June 2001; accepted 28 June 2001

Abstract

A depth-integrated numerical model with grid resolution 500 m has been used to simulate tides around the Lofoten Islands in northern Norway. The model spans more than 3° latitude and covers a sea area of approximately 1.2×10^5 km^2. The fine spatial resolution resolves the important fine scale features of the bottom topography on the shelf and the complex coastline with fjords and islands. Boundary conditions at the oceanic sides of the model domain are obtained by interpolation from a large-scale tidal model covering the Nordic Seas and implemented with the flow relaxation scheme (FRS). The semi-diurnal components M_2, S_2 and N_2 and the diurnal component K_1 are simulated. Harmonic constants for sea level are compared with observations from 21 stations. The best fit is found for the M_2 component with a standard deviation between the observed and modelled amplitude and phase of 2.3 cm and 2.5°, respectively. The standard deviation for the other smaller components ranges between 1.5–2.8 cm and 5.3–16.7°. Current fields from the model are compared with observations in four locations: the Moskenes sound, the Gimsøy channel, the Tjeldsund channel and the Sortland channel. In the Sortland channel, the model predicts a dominant diurnal K_1 current in agreement with observations. © 2002 Published by Elsevier Science Ltd.

Keywords: Tides; Tidal dynamics; Numerical model; High resolution; Tidal currents; Shelf dynamics; Lofoten Islands; Norway

1. Introduction

In the Vestfjorden area (Figs. 1 and 2) inside The Lofoten Islands in northern Norway, the Arcto-Norwegian cod stock spawns from February to March. Here, rich fisheries of great economic importance have occurred since early medieval times. In the 13th century, trading of cod products from Lofoten consolidated the influence and power of the Hanseatic League. The fact that oceanographic elements to a large extent determine the environment for cod spawning and development of eggs and larvae in the Vestfjorden area was realized early (Eggvin, 1932, 1934; Sverdrup, 1952). Since then there have been several studies of the hydrography and the general circulation in the area. The effect of atmospheric forcing was investigated by Furnes and Sundby (1981). McClimans and Nilsen (1991) studied the circulation by a laboratory model. An extensive NATO field measurement campaign, Rocky Water, has also been conducted (Jenserud, 1995, 1996) accompanied by data analysis and model simulations (Melsom, 1997).

*Corresponding author. Tel.: +47-2285-5856; fax: +47-2285-4349.

E-mail address: bjorng@math.uio.no (B. Gjevik).

0278-4343/02/$ - see front matter © 2002 Published by Elsevier Science Ltd.
PII: S0278-4343(01)00078-4

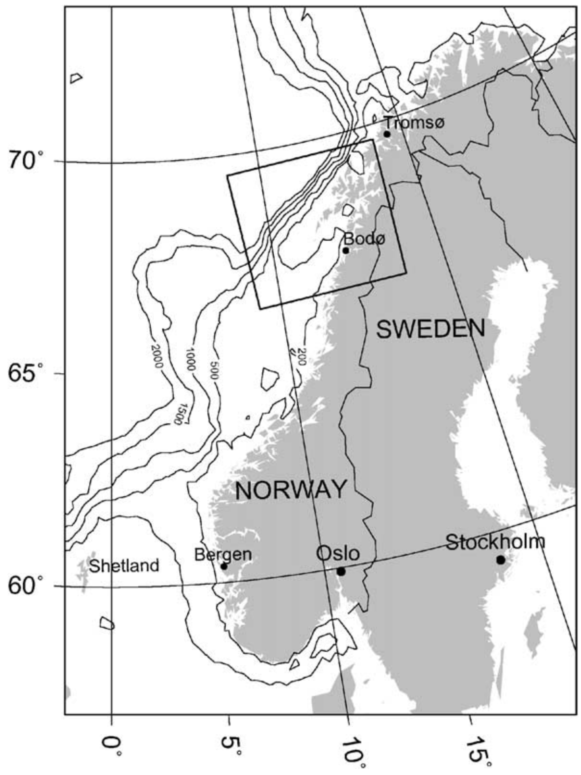

Fig. 1. Map of Norwegian continental shelf with depth contours (meter) and model domain (rectangular box).

Although the tides represent an important part of the current variability in the area, no systematic study of the dynamics of the tides has been reported. Results from coarser grid ($12.5 \times 12.5\ \mathrm{km}^2$) modelling of tides on the Norwegian continental shelf can be found in Gjevik et al. (1990), Gjevik (1990) and some results of the high resolution ($500 \times 500\ \mathrm{m}^2$) model for the main semi-diurnal component M_2 have been published by Gjevik et al. (1997).

Outside The Lofoten Islands, the main semi-diurnal tide is basically a northward propagating wave modified by the topography of the shelf and the coastline. The narrowing of the shelf from a relatively broad shelf south of Lofoten to a narrow shelf on the northern side of the islands and the deflection of the flow due to the island chain itself lead to strong cross-shelf tidal currents near The Lofoten Point (Lofotodden). This local topographic enhancement of the current may play an important role in the transport of eggs and larvae from Vestfjorden to the outer shelf, where they are carried northward by the prevailing shelf edge current (Ådlandsvik and Sundby, 1994; Ommundsen, 2002).

In the Moskenes sound, between The Lofoten Point and the island Mosken, a particularly strong tidal current, Moskstraumen, runs with a speed of up to 5 m/s (Norwegian Hydrographic Service, 1986a). Also, in the sounds between the islands east of Lofotodden, there are strong tidal currents especially in Nappstraumen and Gimsøystraumen. Reports of the strength and power of Moskstraumen inspired the authors Edgar Allen Poe and Jules Verne to fantasize the descriptions of a Maelstrom whirlpool. Historic accounts of The Lofoten Maelstrom can be found in Gjevik et al. (1997) and Gjevik (1998). The fine structure of the current in the area has also been revealed by ERS-1 SAR (Wahl, 1995; Dokken and Wahl, 1995) and by SST signals from AVHRR imagery (Mitchelson-Jacob, 1995). High resolution SAR images also show that wind waves and swell in the area around The Lofoten Point are strongly modified by depth and current refraction (Krogstad, pers. comm. 1999; Neef, 1999).

At certain times of the year, shallow (10–50 m) density stratification occurs in some parts of the area due to fresh water run-off and heating. A deeper density stratification at 150–200 m is present all the year around, particularly in Vestfjorden. This can lead to an internal tide (Nilsen, 1994).

This paper gives a comprehensive presentation and documentation of the results obtained with a high resolution depth-integrated tidal model for the area. The model spans more than 3° latitude and covers a sea area of approximately $1.2 \times 10^5\ \mathrm{km}^2$ (Fig. 1).

With a spatial resolution of 500 m, the model resolves both important fine scale features of the bottom topography on the shelf and the complex coastline with fjords and islands (Fig. 2). This high resolution enables a study of the transition of the tide from basically a northward progressive wave on the shelf to standing oscillations in the fjord basins, and the enhancement of the tidal current in the Moskenes sound and other major currents in the area. For a detailed study of the tide in narrow

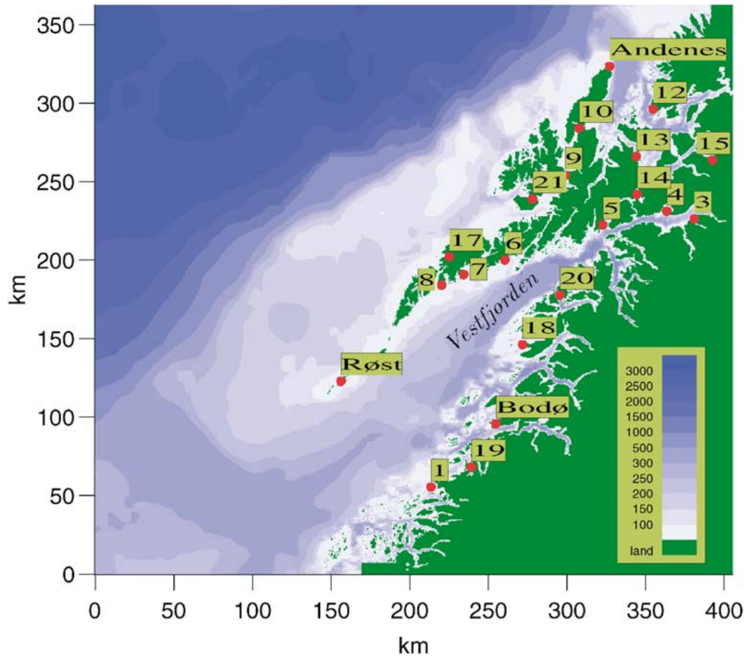

Fig. 2. Model domain with 0.5 km grid resolution. Color depth-scale in meters. The positions of the tidal stations are marked with (red) dots and appropriate map codes.

sounds and fjords, obviously, even finer resolution is required.

High resolution tidal modelling for shelf and coastal areas with complex bathymetry and coastline is a challenging and rapidly developing subject. A review of the state of the art is given by Davies et al. (1997a,b). In particular, the treatment of strong non-linear effects such as turbulence, flow separation and eddy formation is a difficult task (Geyer, 1993; Maddock and Pingree, 1978) which has not been addressed in this paper. Although this model study aims specifically towards an understanding of the dynamics of the tides in The Lofoten area many of the problems accounted here are of wider interest. For example, a similar high resolution model, as used in this study, has recently been developed for the coast of Møre and Trøndelag, Mid-Norway (Moe et al., 2000).

2. Model equations

The depth-integrated shallow water equations are formulated in flux form in a Cartesian coordinate system (x, y, z) with the x- and y-axis in the horizontal plane and the z-axis being vertical:

$$\frac{\partial U}{\partial t} + \frac{\partial}{\partial x}\left(\frac{U^2}{H}\right) + \frac{\partial}{\partial y}\left(\frac{UV}{H}\right) - fV = -gH\frac{\partial \eta}{\partial x} - c_D\frac{\sqrt{U^2+V^2}}{H}\frac{U}{H}, \tag{1}$$

$$\frac{\partial V}{\partial t} + \frac{\partial}{\partial x}\left(\frac{UV}{H}\right) + \frac{\partial}{\partial y}\left(\frac{V^2}{H}\right) + fU = -gH\frac{\partial \eta}{\partial y} - c_D\frac{\sqrt{U^2+V^2}}{H}\frac{V}{H}, \tag{2}$$

where (U, V) are the components of volume flux vector per unit length in the horizontal plane, η the vertical displacement of the sea surface from the mean sea level, $H = H_0 + \eta$ the total depth, H_0 the mean depth, g acceleration of gravity, f the Coriolis parameter, and c_D the drag coefficient of the quadratic bottom shear stress. In addition, the continuity equation reads:

$$\frac{\partial \eta}{\partial t} = -\frac{\partial U}{\partial x} - \frac{\partial V}{\partial y}. \tag{3}$$

The depth mean current velocity is defined by

$$\bar{u} = \frac{U}{H}, \qquad \bar{v} = \frac{V}{H}.$$

In this relatively small model domain, the direct effect of the tide generating forces is assumed to be negligible, and the tidal motion is mainly driven by the boundary input, i.e. sea surface elevation and volume fluxes. For models covering large domains, the tide generating force is known to be important for the diurnal tidal components (Gjevik and Straume, 1989; Davies et al., 1997c). In the present problem, these equations span a wide parameter range from weak tidal flows on the deeper part of the shelf to strong tidal currents near The Lofoten Islands. We introduce a velocity scale u_s, a time scale t_s corresponding to half the tidal period, a tidal amplitude a, a length scale for the spatial variation of the tidal flow l_s and a depth scale h_s. With this scaling we can define the tidal excursion $l_t = u_s t_s$ and Eqs. (1)–(2) can be recast into the dimensionless form:

$$\frac{\partial U}{\partial t} + \alpha\left[\frac{\partial}{\partial x}\left(\frac{U^2}{H}\right) + \frac{\partial}{\partial y}\left(\frac{UV}{H}\right)\right] - \delta V = -\beta H \frac{\partial \eta}{\partial x} - \gamma \frac{\sqrt{U^2+V^2}}{H}\frac{U}{H}, \tag{4}$$

$$\frac{\partial V}{\partial t} + \alpha\left[\frac{\partial}{\partial x}\left(\frac{UV}{H}\right) + \frac{\partial}{\partial y}\left(\frac{V^2}{H}\right)\right] + \delta U = -\beta H \frac{\partial \eta}{\partial y} - \gamma \frac{\sqrt{U^2+V^2}}{H}\frac{V}{H}. \tag{5}$$

The dimensionless form of the continuity equation reads:

$$\frac{\varepsilon \partial \eta}{\alpha \partial t} = -\frac{\partial U}{\partial x} - \frac{\partial V}{\partial y} \tag{6}$$

with $H = H_0 + \varepsilon\eta$. The same symbols are tacitly used here for the dimensionless variables U, V, H and η as in the dimensional equations (1)–(3). The dimensionless parameters are defined by

$$\alpha = \frac{l_t}{l_s}, \qquad \beta = \frac{ga}{u_s^2}\frac{l_t}{l_s}, \qquad \gamma = \frac{c_D l_t}{h_s},$$

$$\delta = f t_s, \qquad \varepsilon = \frac{a}{h_s}. \tag{7}$$

Here α and ε are measures of the importance of the advective terms and the non-linear surface elevation terms, respectively. The parameters β, γ, and δ are scale pressure, bottom friction and rotational effects respectively. In deep water, α, ε and $\gamma \ll 1$ and the equations reduce to the linearized shallow water equation with negligible bottom friction. Near the coast, with strong tidal currents, α, β, γ are of $O(1)$ and all terms in the equation of motion have to be retained. In not too shallow water ($\varepsilon \ll 1$), the left-hand side of Eq. (3) may be neglected rendering a nearly non-divergent volume flux as long as α is of $O(1)$.

In this paper, the performance of a linearized tidal model has been tested and the approximations $\alpha = \varepsilon = 0$ and ε/α of $O(1)$ have been made. Further, the quadratic bottom friction is retained in the model. The equations are then discretized on a C-grid (Mesinger and Arakawa, 1976) with a semi-implicit numerical scheme. This scheme is widely used for depth-integrated ocean models. A discussion of its dispersion and stability properties is given by Martinsen et al. (1979) and Gjevik and Straume (1989). The stability criterion satisfied by the numerical time step Δt is:

$$\Delta t \leqslant \frac{\Delta x}{\sqrt{2gH_{max}}},$$

where Δx is the grid size and $H_{\max}$ is the maximum depth in the model domain.

3. Model setup and boundary conditions

The depth matrix was evaluated on an UTM coordinate grid with $\Delta x = 0.5$ km resolution. Near the coast, average depths for each grid box were read from Norwegian coastal charts most of them with scale 1:50000. Outside the zone covered by the coastal charts, depths are from a bathymetric data base with 500 m spatial resolution provided by the Norwegian Hydrographic Service (NHS) or interpolated from a 4×4 km^2 digital data base. The main part of the model domain is covered by the UTM zone 33W, which for convenience has been extended west of 12°E into UTM zone 32W. Based on the resulting depth matrix of 810×725 grid points (Fig. 2), The Lofoten Islands stretch northeastward from Røst towards Lødingen (map code 5). North of The Lofoten Islands, Vesterålen is located between Stokmarknes and Andenes. The wide fjord south of The Lofoten chain of islands, from Røst and Bodø eastward to Lødingen, is Vestfjorden. The general topography is clearly a relatively wide shelf south of Lofoten and a narrow shelf west of Vesterålen and Andenes.

Boundary conditions for the model were obtained by interpolating surface elevation and volume fluxes from a large-scale model of the Norwegian and the Barents Sea with 25 km grid resolution (Gjevik et al., 1990, 1994). The interior solution was adjusted to the specified boundary conditions with the flow relaxation scheme (FRS), Martinsen and Engedahl (1987). The FRS softens the transition from an exterior solution (here the interpolated data) to an interior solution (model area) by use of a grid zone where the two solutions dominate at each end, respectively. The width of the FRS zone is here taken to be ten grid cells.

Two types of boundary forcing (exterior solutions) have been tested; (i) only surface elevation specified and (ii) both surface and volume fluxes specified. Separate simulations were made for each of the tidal components M_2, S_2, N_2 and K_1. At $t = 0$, the boundary forcing is applied from rest at the oceanic sides of the model domain and the amplitudes grow according to $(1 - \exp(-\sigma t))$. A value of $\sigma = 4.6 \times 10^{-5}\ \mathrm{s}^{-1}$ has been used which implies full effect of boundary conditions after about 12 h.

The simulations begin from rest, i.e., the internal solution $U = V = \eta = 0$. When the simulation reaches 72 h, full fields (all grid points) for current and elevation are stored with half an hour sampling for one additional tidal period. Time series recorded from $t = 0$ at 45 stations within the model domain were examined to ensure that a steady state oscillation was reached. The surface elevation attained steady state rapidly at all stations, but for some stations time series for currents included noise due to the transient start. Longer simulations have been performed, but, for the results present, 72 h was sufficient to reach an acceptable steady state. Harmonic analysis is then performed on the full fields to determine the amplitude and phase for the appropriate tidal component. To investigate the effect of the M_2 current on the bottom friction for K_1, these two components were run together in one simulation. The effect was found to be small. The simulations are normally performed with a bottom friction coefficient of $c_D = 0.003$, but simulations are also done with $c_D = 0$ and 0.006 in order to investigate the effect of bottom friction. Generally, without bottom friction, the simulations will not reach an acceptable steady state within the simulation time, while larger bottom friction ($c_D = 0.006$) tends to increase the gradient of the surface elevation slightly in the narrow straights and sounds between The Lofoten Islands. If not explicitly mentioned, the results presented are from simulations with bottom friction included, single component forcing and boundary condition (i).

4. Results

The calculated harmonic constants for sea level amplitude, h_n, and phase relative Greenwich, g_n, are compared with observations from 21 stations (Tables 1–2, Fig. 2). For Bodø, Narvik, Lødingen, Kabelvåg, Risøyhamna, Andenes, Harstad and Evenskjær (primary stations), the harmonic constants are evaluated from long time series of observed sea level ((NHS), 1998). For the other stations in Tables 1 and 2 (secondary stations), harmonic constants are calculated from shorter time series, typically 2–4 weeks and are, therefore, prone to errors. NHS has given us access to this data set, which previously has not been used for validation of tidal models. For the secondary stations, NHS has also calculated correction factors for amplitude and time of high and low water relative to the nearest primary station. By using these correction factors a set of derived harmonic constants for the secondary stations has also been deduced. Harmonic constants are listed in Tables 1 and 2 for both primary and secondary stations.

Current fields from the model are compared with observations in four locations: The Moskenes sound, the Gimsøy channel, the Tjeldsund channel and the Sortland channel. NHS has provided tidal current data in the areas around Gimsøy (G1–G2) and Sortland (S1–S5), and the University of Bergen has provided the data for the stations in

Table 1
Observed and modelled amplitude (h_n cm) and phase (g_n degree, GMT) of the M_2 and S_2 tide. Model results with prescribed elevation at the open boundaries (*Elevation*) and elevation and fluxes at the open boundaries (*Elev. & flux*)

Station (Map code)	M_2								S_2					
	Observed		Derived		Model elevation		Model elevation & flux		Observed		Derived		Model elevation	
	h_n	g_n	h_n	g_n	h_n	g_n	h_n	g_n	h_n	g_n	h_n	g_n	h_n	g_n
Støtt(1)			86.0	326	82.5	329	84.8	324			29.7	4	27.2	3
Bodø	86.9	331			86.1	332	88.5	327	30.5	9			28.5	6
Narvik(3)	99.3	334			99.6	335	102.2	330	35.3	13			33.1	10
Bogen(4)	94.3	340	99.1	343	99.1	335	101.7	330	38.2	21	34.8	21	32.9	10
Lødingen(5)	93.3	334			96.0	335	98.6	330	32.2	11			31.8	10
Kabelvåg(6)	92.6	334			91.3	335	93.8	330	32.6	13			30.2	10
Stamsund(7)	88.7	335	91.2	336	89.4	336	91.9	331	32.3	12	32.0	14	29.6	11
Ballstad(8)	84.7	338	87.8	335	88.2	337	90.7	332	35.2	15	30.8	13	29.1	11
Sortland(9)	66.3	342	66.9	337	65.6	340	69.3	335	24.4	21	23.5	16	23.0	17
Risøyhamna(10)	67.7	342			65.9	342	70.3	336	21.1	22			23.2	18
Andenes	64.8	341			63.9	342	69.2	336	22.0	20			22.5	18
Skrolsvik(12)	68.5	341	67.1	344	66.2	343	71.7	337	23.2	21	22.1	24	23.3	20
Harstad(13)	69.3	344			67.5	343	73.2	336	23.8	23			23.8	18
Evenskjær(14)	74.0	333			74.3	340	79.7	334	26.1	11			26.2	15
Røkenes(15)	69.9	348	64.6	348	68.7	343	74.4	337	22.1	16	21.3	29	24.3	19
Røst	77.5	334		332	75.9	334	78.1	329	27.6	13		10	25.2	9
Tangstad(17)	62.3	339	65.2	336	63.7	340	66.7	334	24.8	18	22.9	14	22.2	16
Helnessund(18)	90.1	335			88.5	333	91.0	328	32.5	15			29.2	8
Inndyr(19)	85.9	329			84.6	331	87.0	325	30.2	8			27.9	5
Skutvik(20)	98.7	335			92.7	334	95.3	329	36.3	24			30.7	9
Stokmarknes(21)	65.8	338		339	64.9	340	68.4	335	22.1	15		18	22.9	17

The Moskenes sound (L1–L4), Fig. 11, Section 4.2. Wherever data from several depths were available, the depth mean value was used for comparison with model current data from the nearest grid point (Table 3).

4.1. Sea level, semi-diurnal and diurnal components

4.1.1. The M_2 component

Based on contour lines for the M_2 sea level amplitude and phase (Fig. 3), the phase lines are approximately perpendicular to the shelf slope with gradually increasing phases northeastward, showing that the M_2 wave component propagates basically northeastward. Separation between phase lines is also larger north of The Lofoten Islands, where the shelf is narrow, which implies a larger propagation speed than south of Lofoten where the shelf is wider.

The 60 cm amplitude isoline follows the shelf slope and relatively low amplitudes are found in Vesterålen north of The Lofoten Islands where the shelf is narrow. To the south of Lofoten there is almost a linear increase in amplitude from the shelf edge towards the coast. The convergence of contour lines for the amplitude at Røst and The Lofoten Point is due to the scattering of the northward propagating wave by The Lofoten chain of islands. Due to the constraints of the coastline there is also an increase in amplitude by about 24 cm from the mouth of Vestfjorden near Røst eastward towards Narvik (map code 3) at the head of the fjord. Across The Lofoten chain of islands there is a difference in amplitude of 15–30 cm which drives the strong tidal currents in the channels between the islands. The general variation in amplitude and phase observed here is also reproduced to a large extent by an idealized model

Table 2
Observed and modelled amplitude (h_n cm) and phase (g_n degree, GMT) of the N_2 and K_1 tide. Model results with prescribed elevation at the open boundaries (Elevation)

Station (Map code)	N_2						K_1					
	Observed		Derived		Model elevation		Observed		Derived		Model elevation	
	h_n	g_n	h_n	g_n	h_n	g_n	h_n	g_n	h_n	g_n	h_n	g_n
Støtt(1)			17.5	303	17.5	310			8.0	177	10.3	192
Bodø	17.7	307			18.3	313	10.3	194			10.1	195
Narvik(3)	20.3	311			21.1	316	11.2	197			10.4	197
Bogen(4)			20.2	318	21.0	316	12.5	197	11.7	200	10.4	197
Lødingen(5)	20.3	314			20.4	316	10.2	197			10.3	197
Kabelvåg(6)	18.9	311			19.4	317	10.9	195			10.2	198
Stamsund(7)			18.6	311	19.0	317	12.0	194	10.8	196	10.2	197
Ballstad(8)			17.9	310	18.8	318	8.8	190	10.4	196	10.3	198
Sortland(9)	12.7	343	13.6	313	15.4	321	6.7	237	7.9	197	4.5	195
Risøyhamna(10)	16.9	326			15.4	323	3.2	213			5.9	157
Andenes	13.2	317			15.1	323	5.3	184			10.4	178
Skrolsvik(12)	14.3	315	13.6	321	15.6	324	6.8	186	5.7	200	10.4	180
Harstad(13)	14.2	320			15.9	323	5.9	197			10.5	180
Evenskjær(14)	15.1	310			17.3	321	6.5	192			10.6	184
Røkenes(15)			13.1	325	16.2	324	7.4	181	5.5	202	10.5	180
Røst	16.2	310		308	16.3	315	9.3	193		194	8.5	194
Tangstad(17)			13.3	311	14.8	320	9.3	221	7.7	196	7.1	215
Helnessund(18)	17.7	315			18.8	314	11.4	195			10.1	196
Inndyr(19)	17.6	304			17.9	312	8.4	190			10.1	194
Skutvik(20)					19.7	316	10.3	187			10.3	197
Stokmarknes(21)	12.6	339		315	15.1	321	7.5	221		198	5.2	215

Table 3
Parameters for the M_2 current ellipse. For station S4 also K_1 current ellipse. A (cm/s), major half axis; B (cm/s), minor half axis; θ (deg.), orientation of major axis in degrees true; Rot., rotation direction for the current vector (+, clockwise; –, counterclockwise). Depths in meters

Station	Coordinates	Total depth	Sensor depths	Observed (mean)				Model			
				A	B	θ	Rot.	A	B	θ	Rot.
L1	67°44.0′N, 13°17.0′E	198	50, 100, 150	9.6	3.1	64	–	8.1	1.9	69	–
L2	67°47.0′N, 13°00.0′E	91	20, 50, 80	21.2	1.2	291	–	22.0	1.8	277	+
L3	67°53.0′N, 12°33.0′E	132	22, 52, 102	11.6	4.5	112	+	15.2	2.0	155	+
L4	67°59.0′N, 12°15.5′E	194	14, 94, 144	7.3	1.7	355	+	9.0	1.0	344	+
S1	68°34.7′N, 14°55.2′E	22	6, 15	9.8	0.2	85	–	7.3	0.1	99	+
S2	68°34.0′N, 14°55.7′E	14	4	26.9	0.4	25	+	9.9	0.1	316	+
S3	68°36.0′N, 15°10.0′E	69	6, 15	1.7	0.1	53	–	1.8	0.0	45	+
S4	68°43.5′N, 15°26.0′E	30	6, 12	13.0	0.3	10	–	10.2	0.9	2	–
S5	68°55.5′N, 15°36.5′E	30	6, 12	3.5	0.2	198	–	8.5	0.5	194	+
G1	68°16.7′N, 14°17.6′E	24	5, 13	83.3	1.2	216	–	118.0	0.0	0	non
G2	68°15.8′N, 14°15.3′E	11	5	113.9	12.6	41	–	71.0	3.0	68	–
S4 (K_1)	68°43.5′N, 15°26.0′E	30	6, 12	48.5	0.3	8	–	45.6	3.8	359	–

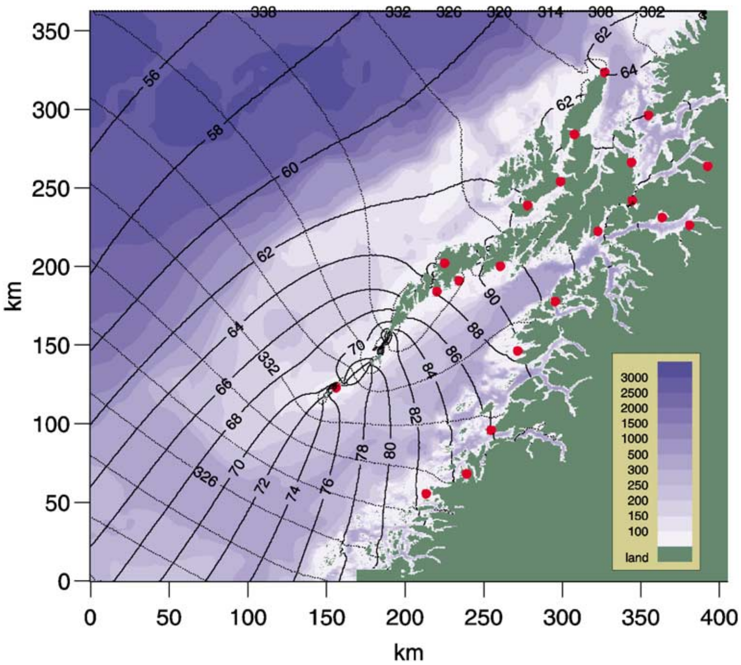

Fig. 3. M_2 sea surface elevation. Isolines for amplitude (solid lines, 2 cm separation) and phase (broken lines, 2° separation). Tidal stations (Table 1) marked by (red) dots. Shading shows depth with scale in legend (meter). Boundary forcing: only surface elevation.

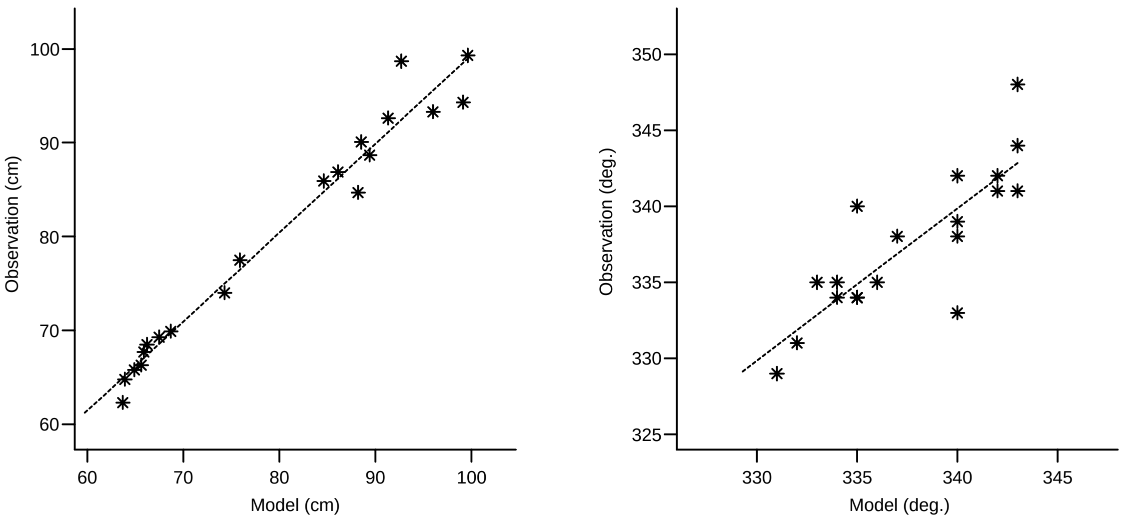

Fig. 4. Scattering diagrams M_2. Comparison between modelled and observed amplitude (left panel) and phase (right panel). The least squares regression line (dashed). The standard deviation estimate between model and observation is 2.29 cm (amplitude) and 2.54° (phase). Boundary forcing: only surface elevation.

with a corresponding transition from a broad to a narrow shelf (Ommundsen and Gjevik, 2000).

By comparing amplitudes and phases with observations, Table 1 and Fig. 4, the best fit is found for the run with prescribed surface elevation at the open boundaries with a standard deviation of only 2.3 cm for amplitude and 2.5° for phase. To obtain this good agreement, minor adjustments

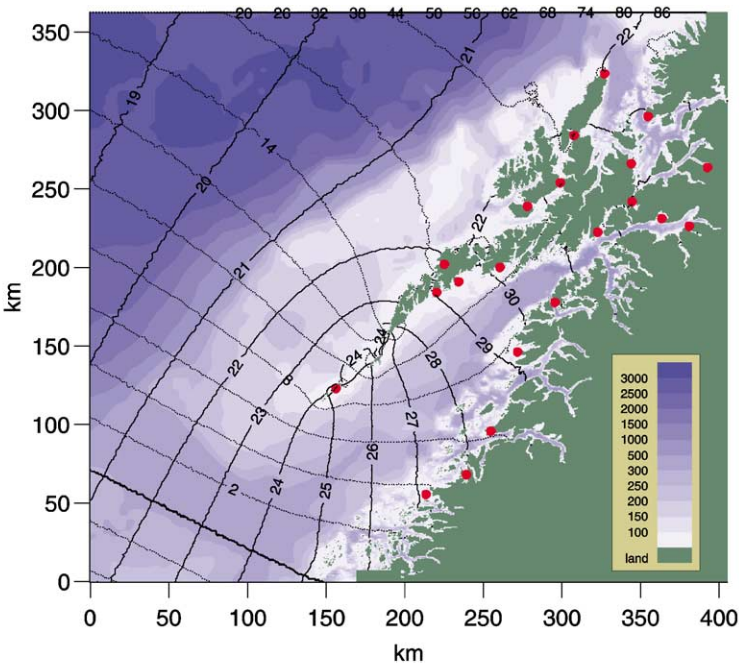

Fig. 5. S_2 sea surface elevation. Isolines for amplitude (solid lines, 1 cm separation) and phase (broken lines, 2° separation). Tidal stations (Table 1) marked by (red) dots. Shading shows depth with scale in legend (meter).

have been made to the surface elevation at the open boundaries. This result indicates that further improvements can be made by using more advanced data assimilation techniques, e.g. Lardner (1993). For the run with surface elevation and fluxes prescribed at the open boundaries the corresponding standard deviations are 3.8 cm and 5.9°.

4.1.2. The S_2 component

The amplitude of the S_2 component is about one-third of the M_2 and the general features of the variation of the amplitude and phase are similar (Fig. 5). The standard deviations between modelled and observed amplitude and phase are 2.8 cm and 5.3°, respectively, for the S_2 simulations with surface elevation prescribed at the open boundary, Table 1 and Fig. 6.

4.1.3. The N_2 component

The amplitude of the N_2 component is about one-fifth of the M_2 and the general features of the variation of the amplitude and phase are similar (Fig. 7). The standard deviations between modelled and observed amplitude and phase are 1.5 cm and 9.5°, respectively, for the N_2 simulations with surface elevation prescribed at the open boundary, Table 2 and Fig. 8.

4.1.4. The K_1 component

The amplitude of sea surface displacement for the largest diurnal component (K_1) is about one-tenth of the M_2. The contour lines for amplitude and phase (Fig. 9) show an interesting picture with small local maxima in amplitude along the shelf slope particularly north of The Lofoten Islands where the shelf is narrow. The separation between these maxima is 25–75 km indicating that the diurnal tide in the area has the structure of shelf waves with short wavelength.

A study of the propagation of diurnal tides by use of a model with idealized bottom topography for the transition from a broad to a narrow shelf shows the occurrence of shelf waves with a short wavelength on the narrow section of the shelf (Ommundsen and Gjevik, 2000). Calculation of

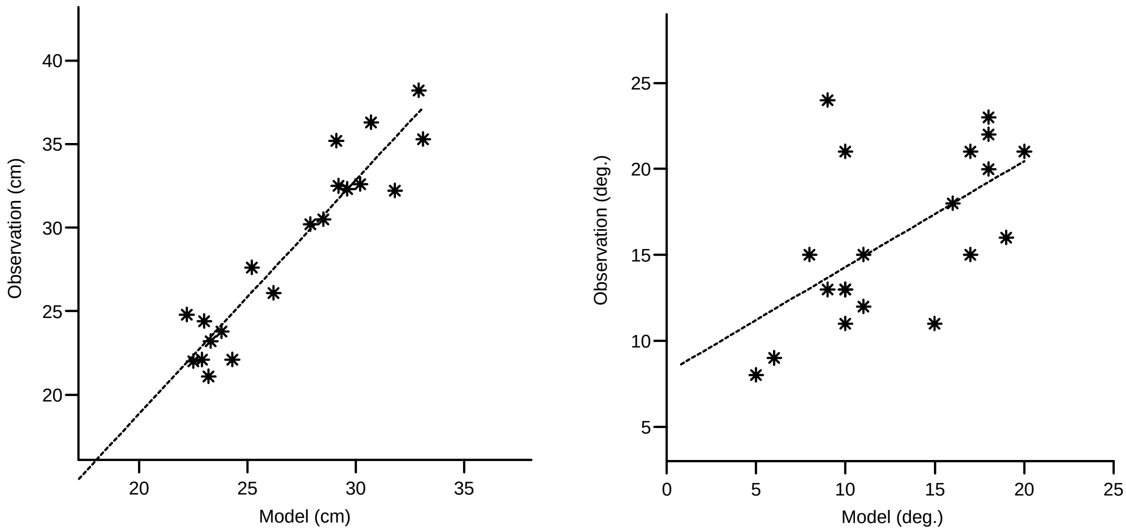

Fig. 6. Scattering diagrams S_2. Comparison between modelled and observed amplitude (left panel) and phase (right panel). The least squares regression line (dashed). The standard deviation estimate between model and observation is 2.8 cm (amplitude) and 5.3° (phase).

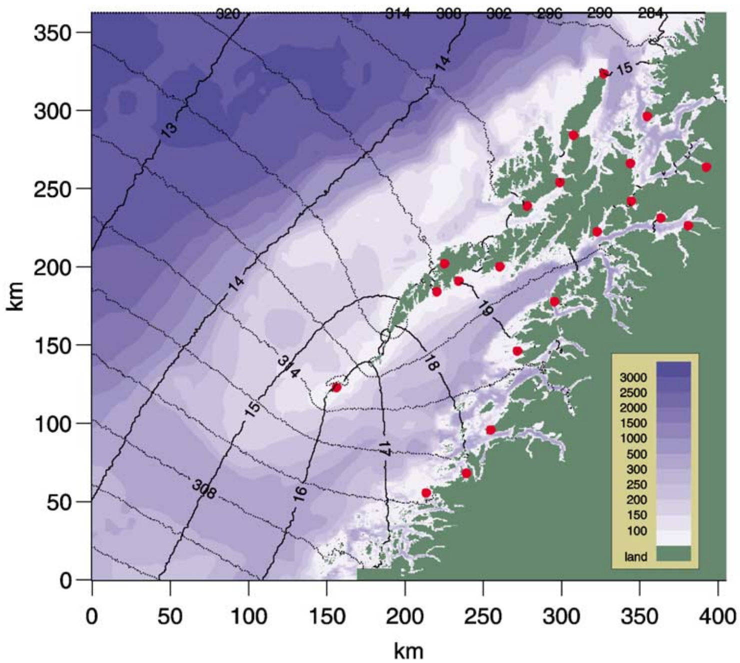

Fig. 7. N_2 sea surface elevation. Isolines for equal amplitude (solid lines, 1 cm separation) and phase (broken lines, 2° separation). Tidal stations (Table 2) marked by (red) dots. Shading shows depth with scale in legend (meter).

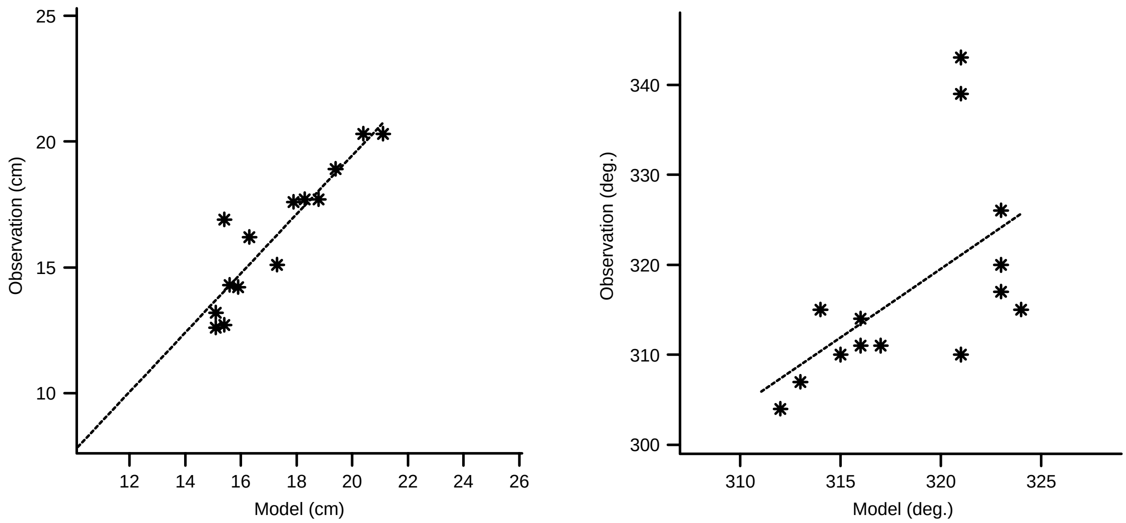

Fig. 8. Scattering diagrams N_2. Comparison between modelled and observed amplitude (left panel) and phase (right panel). The least squares regression line (dashed). The standard deviation estimate between model and observation is 1.5 cm (amplitude) and 9.5° (phase).

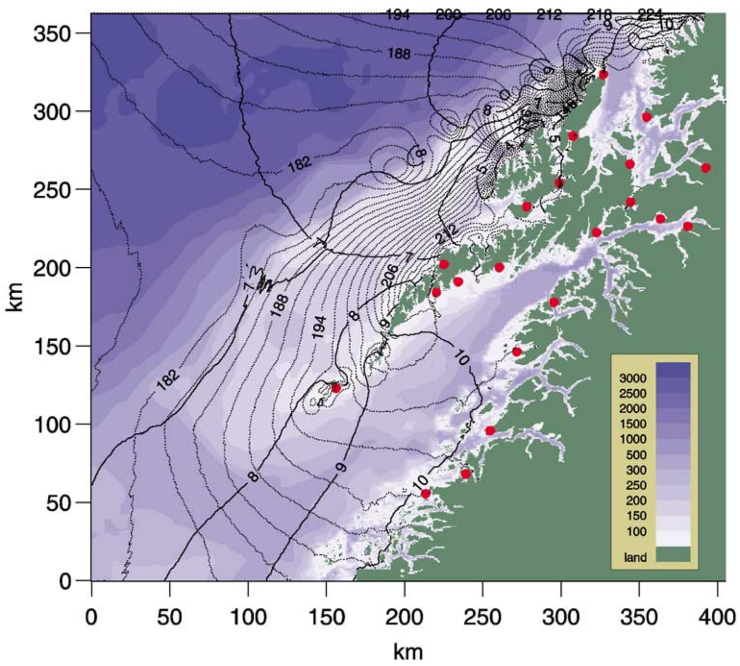

Fig. 9. K_1 sea surface elevation. Isolines for amplitude (solid lines, 1 cm separation) and phase (broken lines, 2° separation). Tidal stations (Table 2) marked by (red) dots. Shading shows depth with scale in legend (meter).

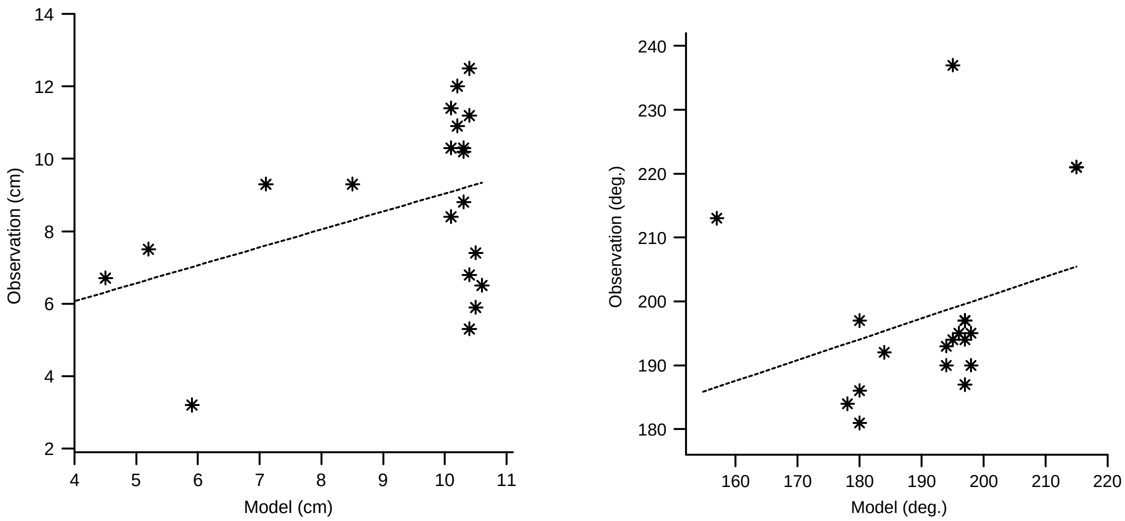

Fig. 10. Scattering diagrams K_1. Comparison between modelled and observed amplitude (left panel) and phase (right panel). The least squares regression line (dashed). The standard deviation estimate between model and observation is 2.5 cm (amplitude) and 16.7° (phase).

modal structure and dispersion properties also show that the narrow shelf north of Lofoten will support shelf wave modes with diurnal period and wavelengths in the range 50–100 km. The importance of shelf wave resonance contribution to K_1 has been reported previously (Gjevik, 1990; Proctor and Davies, 1996).

The regression analysis between observed and modelled amplitude and phase yields a relatively large scatter particularly for phase (Fig. 10). Standard deviation is 2.5 cm for amplitude and 16.7° for phase. Clearly a more optimal set of boundary conditions is required to reproduce the observed amplitude and phase for K_1 with a higher degree of accuracy. A data assimilation procedure would be an interesting next step (e.g. Lardner, 1993).

4.2. Tidal currents

4.2.1. The Moskenes sound

The Moskenes sound, with the small island Mosken in the middle, is located between Værøy (V) and The Lofoten Point (L) (Fig. 12). Here runs the famous Lofoten Maelstrom known worldwide for its strength and for the mystique which surrounds it (Gjevik et al., 1997; Gjevik, 1998). This strong current combined with the background current in the region is an effective mechanism for the transport of eggs, larvae, etc. out of Vestfjorden (Ådlandsvik and Sundby, 1994; Ommundsen, 2002).

The modelled M_2 current is depicted by its peak values and by the current ellipses (Fig. 12). The maximum current is nearly 200 cm/s. The locations of four stations, L1 to L4, with measurements of the tidal current are shown in Fig. 11 and the observed and modelled parameters of the current ellipse are compared in Table 3. The measurements were made over a period of 21 days in April–May 1977 with RCM current recorders. Data are available for three depth levels at each station and depth mean values are shown in the table. The vertical variation is relatively small, indicating that baroclinic effects are of minor importance during this period of measurement. The results of the model are in good agreement with the observations. For station L2, the model predicts clockwise rotation, while observations show counterclockwise rotation. However, it should be noted that L2 is located close to the borderline (Fig. 12) between the areas of opposite rotation.

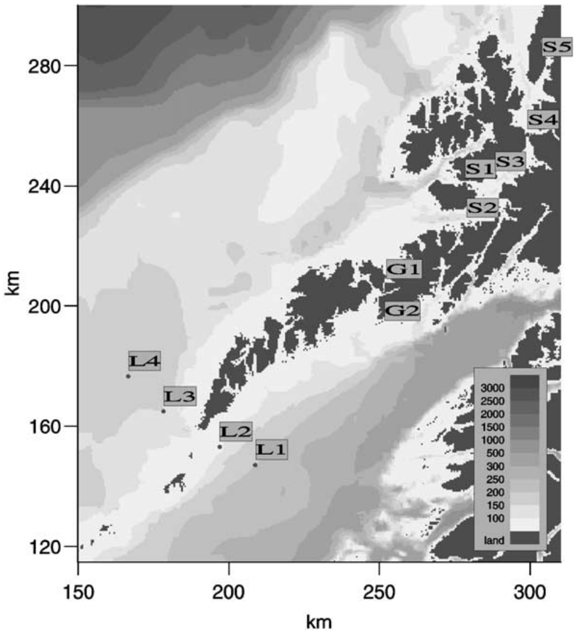

Fig. 11. Locations and map codes for stations with measurements of tidal current. The Moskenes sound (L1–L4), the Gimsøy channel (G1–G2) and the Sortland channel (S1–S5).

Based on the calculated volume flux for M_2, through a cross-section area of $3.1 \times 10^5\ \mathrm{m}^2$ between (V) and (L), the model predicts a mean maximum current of 116 cm/s for the cross-section. Peak outgoing volume flux occurs about 2 h after local high water in agreement with observations.

4.2.2. The Tjeldsund channel

The Tjeldsund channel is a busy sailing route for north and southgoing sea traffic along the coast. For safety reasons it is important to know the current well in this area. Sandtorgstraumen, the main channel northeast of Tjeldøya, is the strongest current (coordinate (343, 240), Fig. 13). The modelled current is examined for its peak values and current ellipses (Fig. 13). A complex pattern is visible in the rotation of the current vector, with local strong currents in Sandtorgstraumen, Balstadstraumen (north of Tjeldøya) and Steinslandstraumen (coordinate (346, 249), Fig. 13).

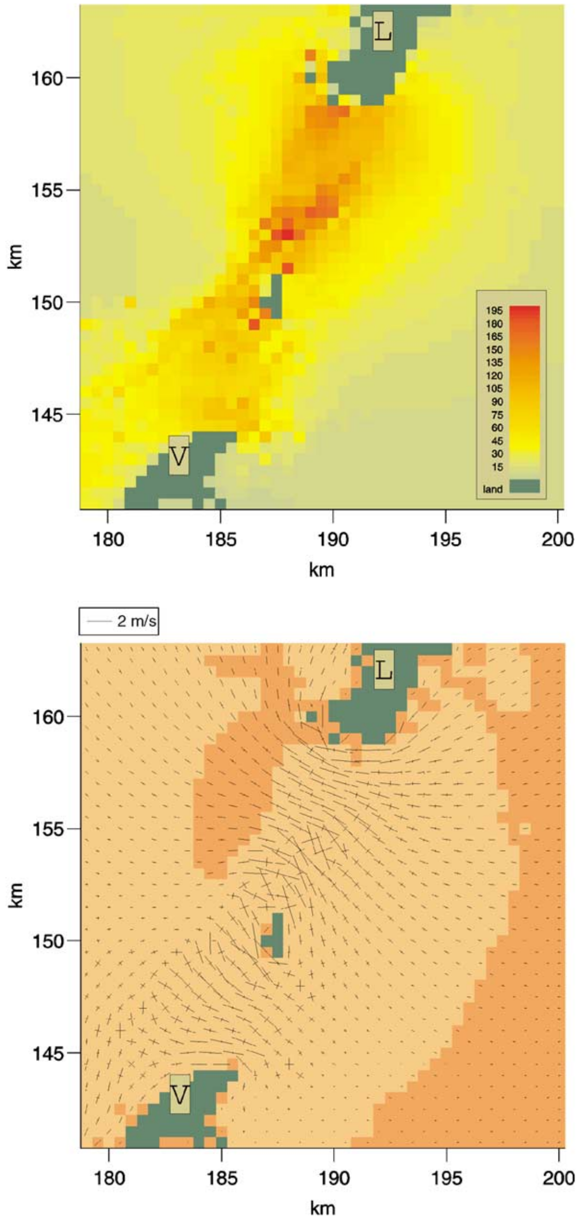

Fig. 12. Upper panel: Maximum M_2 current (major half axis) in the area between The Lofoten Point (L) and Værøy (V). Color scale in cm/s, legend. Lower panel: Tidal ellipse and rotation of the M_2 current vector. Bright shadowing clockwise rotation, darker shadowing counterclockwise. The crosses show the major and minor axes.

According to the pilot book, Norwegian Hydrographic Service (1986b), a maximum northward current in Sandtorgstraumen occurs approxi-

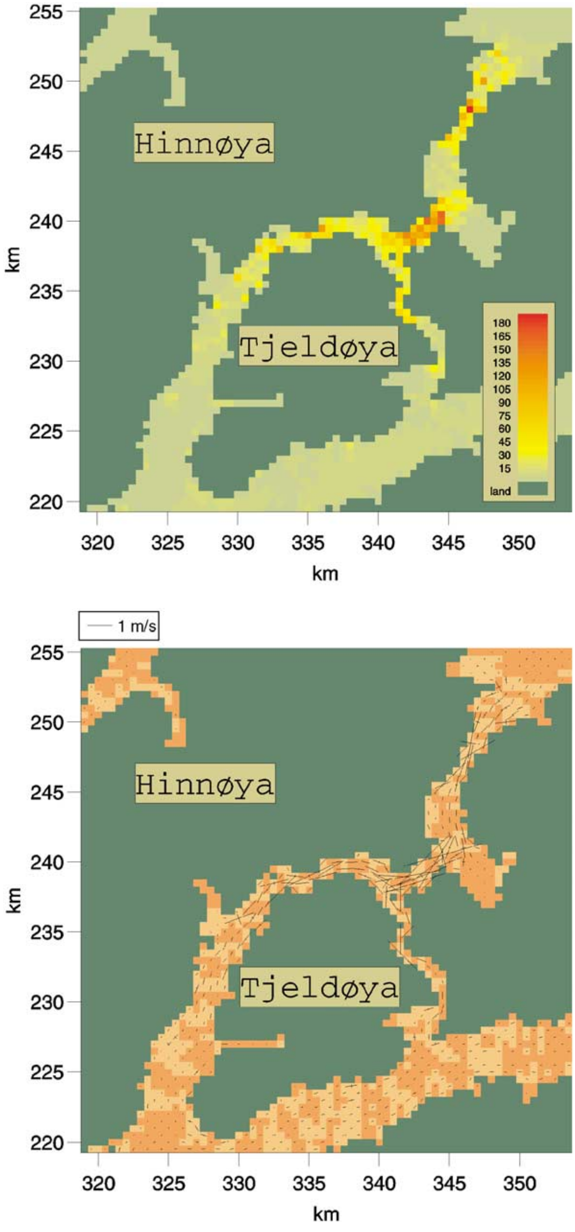

Fig. 13. Upper panel: Maximum M_2 current (major half axis) in the Tjelsund channel. Color scale in cm/s, legend. Lower panel: Tidal ellipse and rotation of the M_2 current vector. Bright shadowing clockwise rotation, darker shadowing counterclockwise. The crosses show the major and minor axes.

mately at high water running with a maximum speed of 206 cm/s at spring. Based on the calculated volume flux for M_2 the model predicts a maximum northward current, running with 168 cm/s, approximately 1 h after high water (Fig. 14). Correspondingly, the combined effect of M_2 and S_2 is found to be 228 cm/s and $M_2 + S_2 + N_2 + K_1$ gives 314 cm/s.

4.2.3. The Sortland channel

Sortlandsundet is the name of the narrow channel between Sortland and Hinnøya, Fig. 15. Based on measurements by NHS, from two measurement periods, the current field in Sortlandsundet is characterized by a strong K_1 component. At station S4, located in the center of Sortlandsundet, the K_1 major half axis was measured to be about 3 times the M_2 major half axis for both periods. Data from April–June, 1993 are shown in Table 3. In the data from February–March campaign, the current amplitudes are about 30% lower. In both periods, the depth variation of the current is small. Normally, the M_2 current dominates along the Norwegian coast. The modelled current is depicted by its peak values and current ellipses for, respectively, the M_2 and K_1 components in Figs. 15 and 16. Five stations S1–S5, with measurements of the tidal current, are examined in Fig. 11 and ellipse parameters for M_2 and K_1 (station S4) are listed in Table 3. Observed and modelled current speed is in good agreement for all stations except S2, and captures the dominant K_1 component in station S4.

The peak volume fluxes for the two components are 2888 and 12 546 m^3/s, respectively. With a cross-section area of 26×10^4 m^2 for Sortlandsundet, the corresponding peak mean current is 11 and 48 cm/s, respectively, which agrees well with observations.

The ratio between the major axis for K_1 and M_2 (Fig. 17) reveals a dominant diurnal current component on a wide area of the shelf north of Lofoten. In some cases, e.g. for north of Vestvågøy, the M_2 current is very small leading to a large ratio although K_1 is not particularly large. The situation in Sortlandsundet seems to be unique since both the M_2 and K_1 components are relatively large. The large diurnal current in the area is clearly an effect of transformation of the

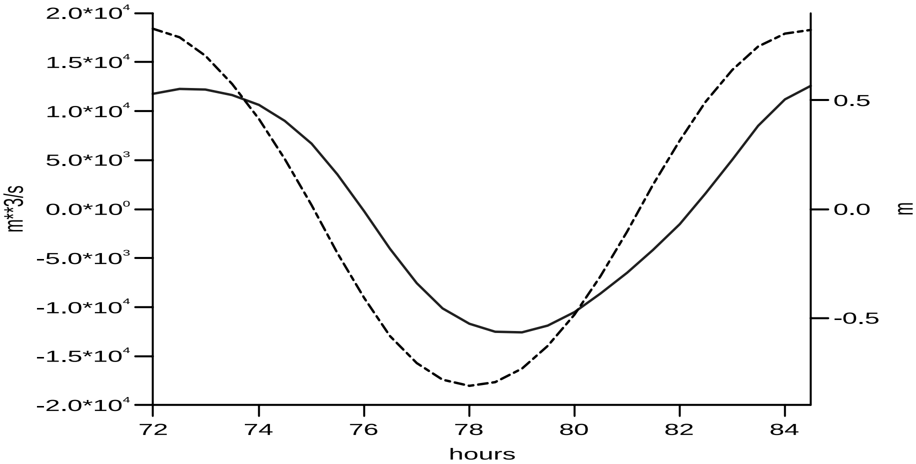

Fig. 14. Volume flux (solid) and sea surface elevation (dotted) in Sandtorgstraumen, cross-section between coordinates (342, 241) and (345, 237). The total area of this cross-section is 7500 m^2 leading to a mean peak northward current of 168 cm/s.

diurnal tide into shelf waves along the narrow shelf northwest of Lofoten (Section 4.1.4).

A dominant diurnal current component has been reported (Lønseth and Schjølberg, 1993) near the shelf edge in Vesterålen at two closely located stations, water depths 450 and 517 m, respectively. The positions (69°N, 13°30′E) are approximately located at a map coordinate (222, 288). Current was measured with RCM currentmeters during 4- and 9-month periods from June 1992 to March 1993. At all depth levels, K_1 current is larger than M_2 and the variation with depth is small except for records near the sea bed. Measured mean values for depths less than 300 m for the major half axes for M_2 and K_1 are 1.2 and 2.0 cm/s, respectively. The modelled values for the major axes for M_2 and K_1 in this location are 1.1 and 5.5 cm/s, respectively.

4.2.4. The Gimsøy channel

The Gimsøy channel is located between The Lofoten islands Vestvågøy and Austvågøy with the island Gimsøy in the middle. A strong current, Gimsøystraumen, runs in the narrow channel between Gimsøy and Austvågøy and another current, Sundklakkstraumen, in the narrow channel between Gimsøy and Vestvågøy.

The modelled current is depicted by its peak values and by the current ellipses (Fig. 18). A complex pattern is visible in the rotation of the current vector, with strong currents in Sundklakkstraumen and Gimsøystraumen. The two available stations with current measurements, G1 and G2 (Table 3, Fig. 11), are located in Gimsøystraumen. The model results (Table 3) are comparable to the observed values, but, with a 500 m grid resolution, representative grid positions for the stations are difficult to obtain in the narrow channel. Data from the nearest grid point with approximately the same depth as in the measurement station have been used.

The pilot book, Norwegian Hydrographic Service (1986a), predicts maximum northward current in Gimsøystraumen approximately 1 h after high water running with a speed of 231 cm/s at spring. Based on the calculated volume flux for M_2, the model predicts a maximum northward current in Gimsøystraumen of 115 cm/s (Fig. 19) approximately 1 h after high water. Correspondingly the combined effect of M_2 and S_2 is 158 cm/s while $M_2 + S_2 + N_2 + K_1$ gives 233 cm/s.

The modelled maximum M_2 current is in fair agreement with observations from stations G1 and G2, Table 3. Based on the calculated volume flux in Sundklakkstraumen between coordinates

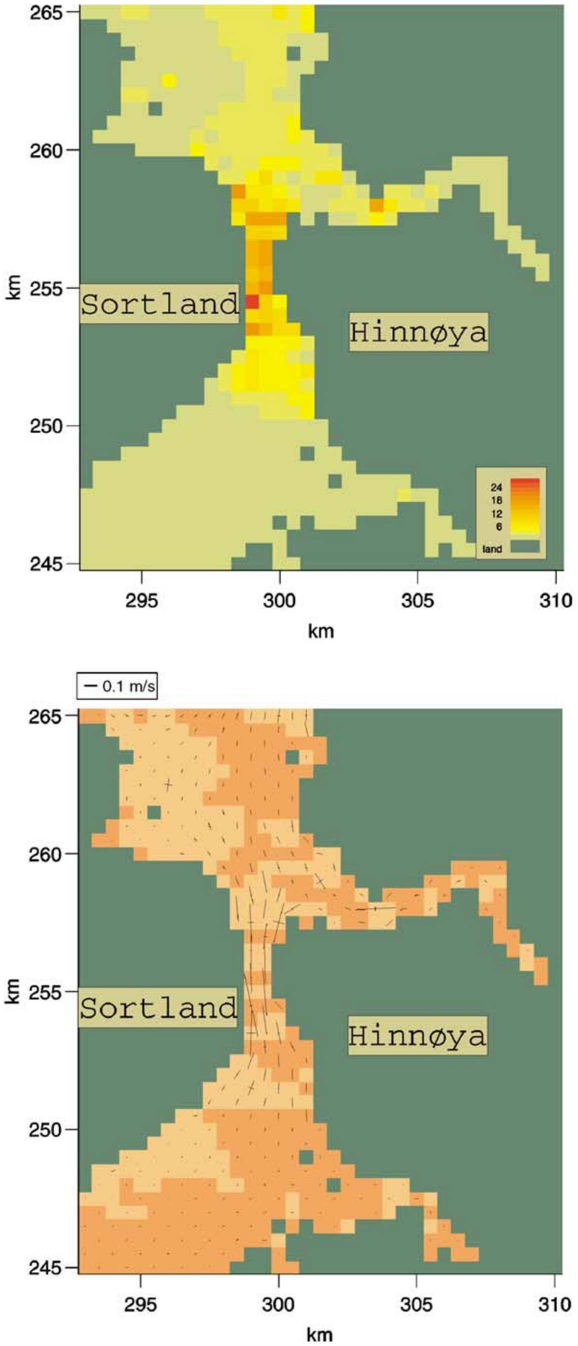

Fig. 15. Upper panel: Maximum M_2 current (major half axis) in Sortlandsundet between Sortland and Hinnøya. Color scale in cm/s, legend. Lower panel: Tidal ellipse and rotation of the M_2 current vector. Bright shadowing clockwise rotation, darker shadowing counterclockwise. The crosses show the major and minor axes.

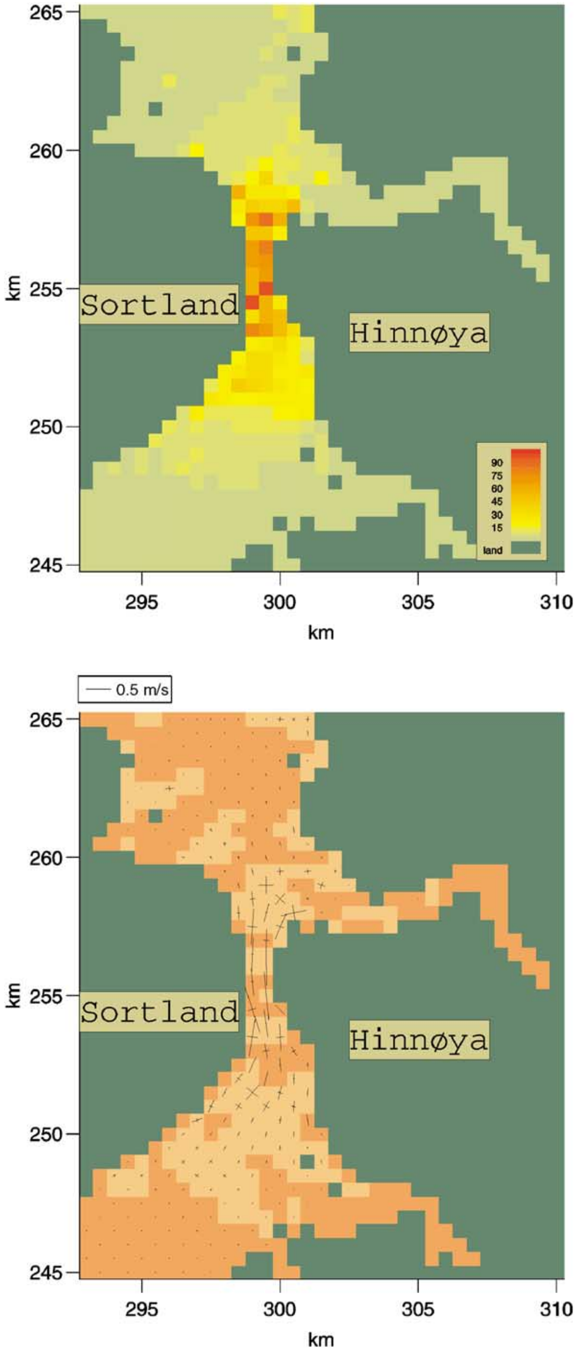

Fig. 16. Upper panel: Maximum K_1 current (major half axis) in Sortlandsundet. Color scale in cm/s, legend. Lower panel: The rotation of the K_1 current vector. Bright shadowing depicts region with clockwise rotation, darker shadowing counterclockwise rotation. The crosses show the major and minor axes.

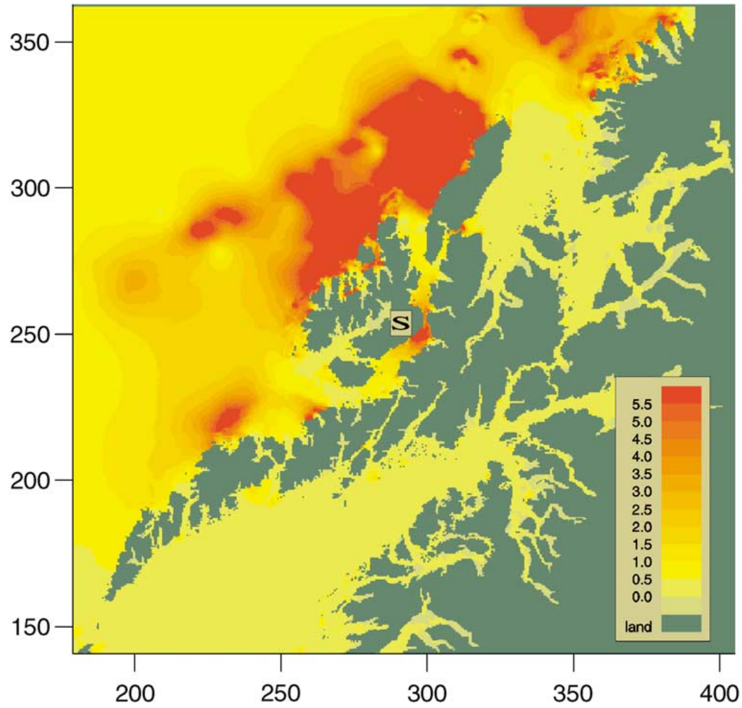

Fig. 17. The ratio between the major axes of the current ellipses for the K_1 and M_2 components. Sortlandsundet (S) in the center. Color scale in legend.

(245, 207) and (250, 207), a slightly slower M_2 mean current of 1.0 m/s is found.

The major axis of the M_4 component (period 6.2 h), which is due to non-linear interaction, is measured to be 13.6 cm/s at 5 m depth at station G1. In the model with only non-linear bottom friction terms included, a smaller M_4 current of about 4 cm/s is found in the same location. This indicates that non-linear advection terms are of importance in this region.

4.2.5. Visual observation of current shift

During the period 12–14 July 1996, one of the authors (Gjevik) observed visually the shift in direction of the tidal current in Gimsøystraumen and Sundklakkstraumen, (see Section 4.2.4). Similar observations were also made in two other channels, Nappstraumen and Sundstraumen, further west in Lofoten. The times of the current shift, i.e. slack water, were estimated following the drift of markers (sea weed, jellyfish, etc.) floating on the surface. In Gimsøystraumen and Sundklakkstraumen, the bridges provided convenient platforms for the observations. The drift of the markers could not be estimated well unless the current was above a certain level. The fact that the current did not turn simultaneously across the channel made it difficult to estimate the exact time of the turning. In most cases, it was only possible to determine the time of turning within an interval of 30–60 min for slack water. The observations are compared with the predicted time of current shift in the channels from a model simulation including all four components M_2, S_2, N_2, and K_1 (Table 4). In view of the relatively large uncertainty in the observational data, the agreement with model prediction is good.

5. Concluding remarks

The high resolution depth-integrated model is found to reveal important features of the dynamics

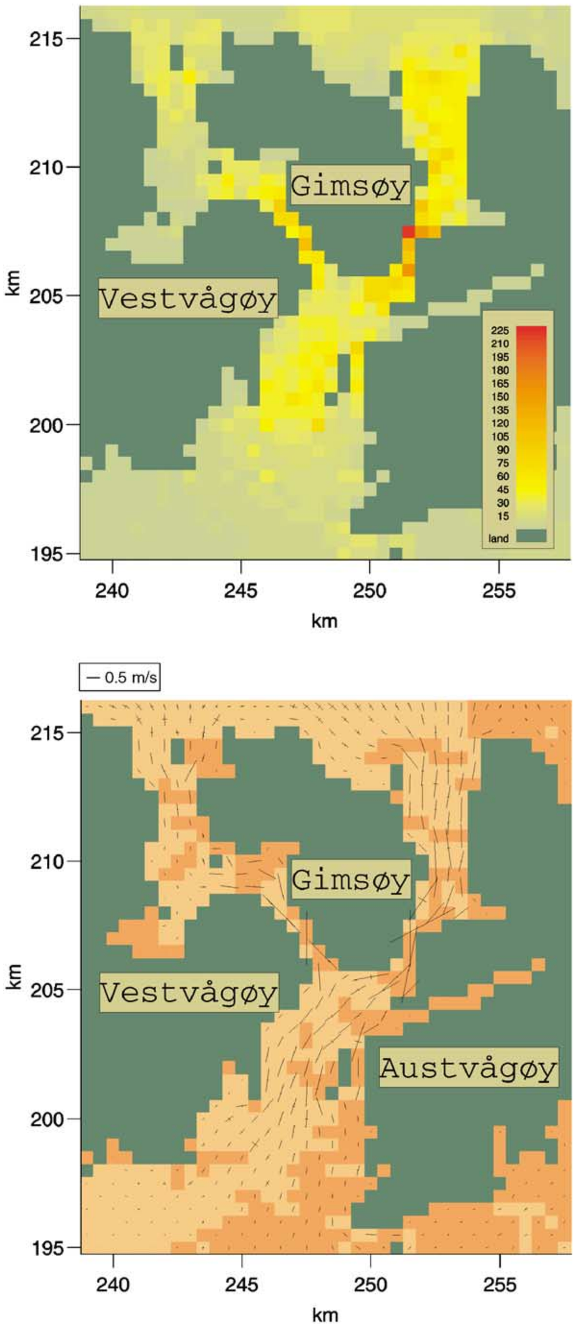

Fig. 18. Upper panel: Maximum M_2 current (major half axis) in Gimsøystraumen. Color scale in cm/s, legend. Lower panel: Tidal ellipse and rotation of the M_2 current vector. Bright shadowing clockwise rotation, darker shadowing counterclockwise. The crosses show the major and minor axes.

of the tides around The Lofoten Islands. Due to the bottom topography of the shelf and the geometry of the coastline, a characteristic variation in tidal amplitude is found with relatively larger amplitudes south of the islands than north of the islands where the shelf is narrow. This large-scale variation in sea level amplitude and phase for the three semi-diurnal constituents M_2, S_2, and N_2 is in good agreement with observations. For the main diurnal component (K_1), with sea level amplitude of about one-tenth of the dominant semi-diurnal component (M_2), the difference between model and observation is large. The simulations show that the diurnal tide transforms into shelf wave modes on the narrow shelf north of The Lofoten Islands leading to a dominance of the diurnal current component in this area of the shelf and in some channels along the coast. This interesting result is also confirmed by measurements. Although the agreement between model and observation is generally very good, there are systematic deviations, specially for the diurnal component, which can be improved with the use of data assimilation techniques.

The success of the model in predicting the speed and the time of shift of the current in main channels between The Lofoten Islands shows that the local tidal conditions are to a large extent determined by the large-scale dynamics of the tide in deep water where non-linear effects are negligible. To simulate the current field in channels with strong tidal current turbulence, flow separation and eddy formation need to be represented in a more realistic way in the model. This will require the use of an adaptive grid or nesting of finer grid models in certain areas. Although the current data used for model validation in this study show a little effect of density stratification, it may be important. This needs to be investigated in future model studies.

Despite these limitations, the results of the simulations with this barotropic tidal model stand in their own right and could serve as a starting point for more advanced modelling exercises and as a guidance for future measurement programs.

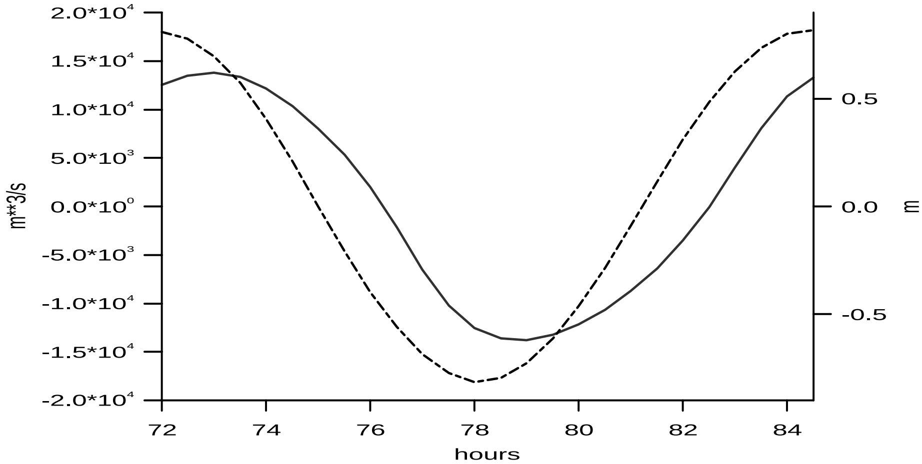

Fig. 19. Volume flux (solid) and sea surface elevation (dotted) in Gimsøystraumen, cross-section between coordinates (250, 207) and (253, 207). The area of this cross-section is 12,000 m^2 leading to a mean peak northward current of 115 cm/s.

Table 4
Observed and modelled time (UTC) for slack water 12–14 July 1996

Location	12 July		13 July		14 July	
	Mod Time Dir.	Obs Time	Mod Time Dir.	Obs Time	Mod Time Dir.	Obs Time
Gimsøystraumen (226, 206)	1330 NE→SW 1945 SW→NE	1300–1400 1910–1930	0845 SW→NE	0805–0835		
Sundklakkstraumen (247, 207)	1230 N→S 1900 S→N	1200–1300 1930–1925	0745 S→N	0725–0850		
Nappstraumen (218, 194)			1445 NE→SW 2045 SW→NE	1430–1445 2000–2125		
Sundstraumen (205, 182)					1345 NW→SE 1945 SE→NW	1240–1320 –2100

Acknowledgements

We are grateful to the Norwegian Hydrographic Service for providing access to their data archive on sea level and current records and to S. Sundby at Institute of Marine Research Bergen and to S. Myking at Geophysical Institute University of Bergen for processing data records of current from the Moskenes sound for us. The assistance by O. Høvik, T. Sjølie, I. Fossum, J. Gjevik and E. Onsum in generating a high resolution depth matrix for the area is greatly appreciated. This work has also received support from the Research Council of Norway, contracts 109228/122 MAR-EMI and 133102/431 BeMatA program.

References

Ådlandsvik, B., Sundby, S., 1994. Modelling the transport of cod larvea from The Lofoten area. ICES Marine Science Symposium on Cod and Climate Change (Reykjavik, 1993) 198, 379–392.

Davies, A.M., Jones, J.E., Xing, J., 1997a. Review of recent developments in tidal hydrodynamic modeling. I: spectral models. Journal of Hydraulic Engineering 123 (4), 278–292.

Davies, A.M., Jones, J.E., Xing, J., 1997b. Review of recent developments in tidal hydrodynamic modeling. II: turbulence energy models. Journal of Hydraulic Engineering 123 (4), 293–302.

Davies, A.M., Kwong, S.C.M., Flather, R.A., 1997c. A three-dimensional model of diurnal and semidiurnal tides on the European shelf. Journal of Geophysical Research 102 (C4), 8625–8656.

Dokken, T.S., Wahl, T., 1995. ERS-1 SAR observations of tidal currents in the Moskenes Sound. Report 04882, Forsvarets Forskningsinstitutt. Kjeller, Norway.

Eggvin, J., 1932. Vannlagene på fiskefeltene. Årsberetning Norges Fiskerier 2, 90–95.

Eggvin, J., 1934. De oceanografiske forhold i Vestfjorden og deres sammenheng med lofotfisket 1933. Årsberetning Norges Fiskerier 2, 94–102.

Furnes, G.K., Sundby, S., 1981. Upwelling and wind induced circulation in Vestfjorden. In: Sætre, R., Mork, M. (Eds.), The Norwegian Coastal Current, Volume 1 of Proceedings from the Norwegian Coastal Current Symposium, Geilo. University of Bergen, Norway, pp. 152–177.

Geyer, W.R., 1993. Three-Dimensional tidal flow around headlands. Journal of Geophysical Research 98 (1), 955–966.

Gjevik, B., 1990. Model simulations of tides and shelf waves along the shelves of the Norwegian–Greenland–Barents Seas. In: Davies, A.M. (Ed.), Modelling Marine Systems, Volume 1. CRC Press Inc., Boca Raton, FL, pp. 187–219.

Gjevik, B., 1998. Moskstraumen myter, diktning og virklighet. Annual proceeding of The Norwegian Academy of Science and Letters, Oslo, Norway.

Gjevik, B., Moe, H., Ommundsen, A., 1997. Sources of the Maelstrom. Nature 388 (28), 837–838.

Gjevik, B., Nøst, E., Straume, T., 1990. Atlas of tides on the shelves of the Norwegian and the Barents Seas. Report FoU-ST 90012, Department of Mathematics, University of Oslo.

Gjevik, B., Nøst, E., Straume, T., 1994. Model simulations of the tides in the Barents Sea. Journal of Geophysical Research 99 (C2), 3337–3350.

Gjevik, B., Straume, T., 1989. Simulations of the M_2 and the K_1 tide in the Nordic Seas and the Artic Ocean. Tellus A (41), 73–96.

Jenserud, T., 1995. Rocky Water 93/10B-A synoptic CTD data set. FFI/Notat 95/00749, The Norwegian Defense Research Establishment.

Jenserud, T., 1996. Synoptic CTD measurements in Vestfjorden. FFI/Rapport 96/04160, The Norwegian Defense Research Establishment. 70pp.

Lardner, R.W., 1993. Optimal control of open boundary conditions for a numerical tidal model. Computer Methods in Applied Mechanics and Engineering 102, 367–387.

Lønseth, L., Schjølberg, P., 1993. Miljøforhold i Norskehavet; Vesterålen. Year Report 49570, Oceanor, Trondheim, Norway.

Maddock, L., Pingree, R.D., 1978. Numerical simulation of the Portland tidal eddies. Estuarine and Coastal Marine Science 6, 353–363.

Martinsen, E.A., Engedahl, H., 1987. Implementation and testing of a lateral boundary scheme as an open boundary condition in a barotropic ocean model. Coastal Engineering 11, 603–627.

Martinsen, E.A., Gjevik, B., Røed, L.P., 1979. A numerical model for long barotropic waves and storm surges along the western coast of Norway. Journal of Physical Oceanography 9 (6), 1126–1138.

McClimans, T.A., Nilsen, J.H., 1991. Laboratory simulations of ocean circulation around Lofoten from October 1982 to June 1984. Report STF60 A91027, SINTEF/NHL, Trondheim, Norway, 7034 Trondheim, Norway.

Melsom, A., 1997. Ocean circulation in Vestfjorden. Research Report 57, Norwegian Meteorological Institute, P.O. Box 43 Blindern, Oslo, Norway.

Mesinger, F., Arakawa, A., 1976. Numerical methods used in atmospheric models. Global Atmosphere Research Programme (GARP) Publ. Ser. WMO 17, 64pp.

Mitchelson-Jacob, E.G., 1995. The oceanography of Vestfjorden, Norway based on the interpretation of 12 years of AVHRR imagery (1981–1992). Report U95-3, University of Wales, Bangor, Marine Science Laboratories, Menai Bridge, Wales, UK.

Moe, H., Gjevik, B., Ommundsen, A., 2000. A high resolution tidal model for the coast of Møre and Trøndelag, Mid Norway. Preprint Series, Department of Mathematics, University of Oslo.

Neef, B.J., 1999. Ocean wave analysis of Moskstraumen. Department of Mathematical Sciences, 75800 Mathematical Project 2, NTNU, Norway.

Nilsen, J.H., 1994. An experimental study of internal tidal amphidromes in Vestfjorden. Ph.D. Thesis, The Norwegian Institute of Technology, Trondheim, Norway.

Norwegian Hydrographic Service, 1986a. Pilot books for the Norwegian coast, 4th Edition. Number 5 in Den Norske Los. Stavanger, Norwegian Hydrographic Service, Norway; ISBN 82-90653-02-6.

Norwegian Hydrographic Service, 1986b. Pilot books for the Norwegian coast, 4th Edition. Number 6 in Den Norske Los. Stavanger, Norwegian Hydrographic Service, Norway; ISBN 82-90653-05-0.

Norwegian Hydrographic Service, 1998. Tide tables for the Norwegian coast and Svalbard, 61st Edition. Stavanger, Norwegian Hydrographic Service, Norway.

Ommundsen, A., 2002. Models of cross shelf transport introduced by The Lofoten Maelstrom. Continental Shelf Research 22, 93–113.

Ommundsen, A., Gjevik, B., 2000. Scattering of tidal Kelvin waves along shelves which vary in their lengthwise direction. Preprint Series, Department of Mathematics, University of Oslo.

Proctor, R., Davies, A.M., 1996. A three dimensional hydrodynamic model of tides off the north-west coast of Scotland. Journal of Marine Systems 7, 43–66.

Sverdrup, H.U., 1952. Havlære. Fabritius & Sønners Forlag, Oslo, Norway.

Wahl, T., 1995. The Maelstrøm seen from space. Nordic Space Activities 2–3, 22–23.